

OPEN

Hepatospecific ablation of p38 α MAPK governs liver regeneration through modulation of inflammatory response to CCl₄-induced acute injury

Manon Fortier^{1,2}, Mathilde Cadoux^{1,2}, Nadia Boussetta², Sandrine Pham^{1,2}, Romain Donn  ^{1,2}, Jean-Pierre Couty^{1,2}, Chantal Desdouets^{1,2} & S  verine Celton-Morizur^{1,2} 

Mammalian p38 α MAPK (Mitogen-Activated Protein Kinase) transduces a variety of extracellular signals that regulate cellular processes, such as inflammation, differentiation, proliferation or apoptosis. In the liver, depending of the physiopathological context, p38 α acts as a negative regulator of hepatocyte proliferation as well as a promotor of inflammatory processes. However, its function during an acute injury, in adult liver, remains uncharacterized. In this study, using mice that are deficient in p38 α specifically in mature hepatocytes, we unexpectedly found that lack of p38 α protected against acute injury induced by CCl₄ compound. We demonstrated that the hepatoprotective effect alleviated ROS accumulation and shaped the inflammatory response to promote efficient tissue repair. Mechanistically, we provided strong evidence that Ccl2/Ccl5 chemokines were crucial for a proper hepatoprotective response observed secondary to p38 α ablation. Indeed, antibody blockade of Ccl2/Ccl5 was sufficient to abrogate hepatoprotection through a concomitant decrease of both inflammatory cells recruitment and antioxidative response that result ultimately in higher liver damages. Our findings suggest that targeting p38 α expression and consequently orientating immune response may represent an attractive approach to favor tissue recovery after acute liver injury.

Acute liver injuries (ALI) can be caused by drug, virus, alcohol, toxic chemical, and several other factors and is a common pathway to many liver diseases^{1–5}. The pathogenesis of ALI involves inflammation, oxidative stress coupled to the production of reactive oxygen species (ROS) and hepatocyte cell death (apoptosis and necrosis)^{6–9}. ALI are characterized by a rapid resolution and a complete restitution of normal organ architecture and function after the elimination of the cause. However, in some cases, ALI may progress to chronic liver injury, hepatic fibrosis, or even hepatocellular carcinoma^{10,11}. Therefore, searching for new therapeutic strategies improving recovery process is critical for a better handling of liver diseases.

p38 Mitogen-activated protein kinases (MAPKs) are essential for the cellular response against injury by integrating a plethora of pathways including growth, inflammation, metabolism and apoptosis^{12–14}. Among all p38 isoforms, p38 α (MAPK14) is the best characterized and expressed in most cell types¹⁵. As mice lacking p38 α isoform die in utero due to angiogenic defects in the placenta and peripheral vessels^{16–18}, mice models harboring tissue-specific deletion of p38 α have been developed. During liver regeneration following partial hepatectomy, mice with specific ablation of p38 α in hepatocytes early in life exhibited enhanced hepatocyte proliferation revealing that p38 α acts as an inhibitor of hepatocyte proliferation by antagonizing the activity of the JNK–c-Jun pathway^{19–21}. By contrast, liver-specific ablation of p38 α during chronic biliary cirrhosis reduced hepatocyte cell growth, caused mitotic blockade and cytokinesis failure impairing dramatically mice lifespan²². Studies in

¹Centre de Recherche des Cordeliers, INSERM, Sorbonne Universit  , USPC, Universit   Paris Descartes, Universit   Paris Diderot, Team (Proliferation, Stress and Liver Physiopathology), F-75006, Paris, France. ²Institut Cochin, INSERM U1016, CNRS UMR8104, Paris Descartes University, Paris, France. Chantal Desdouets and S  verine Celton-Morizur contributed equally. Correspondence and requests for materials should be addressed to S.C.-M. (email: severine.morizur@inserm.fr)

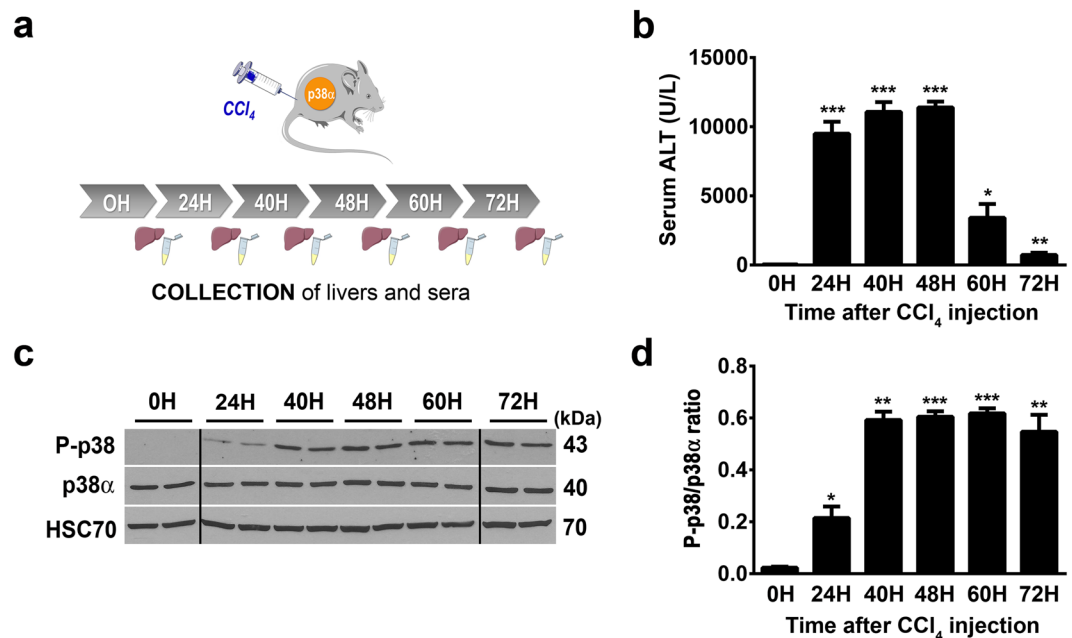


Figure 1. p38 α is activated during acute CCl₄ exposure. (a) Schematic representation of experimental procedure for CCl₄ injection in control mice (CTR). (b) Average alanine aminotransferase (ALT) levels in CTR sera samples before (0H) and after (24H to 72H) CCl₄ exposure. Data represent the mean \pm SEM ($n \geq 6$ per group); * $p < 0.05$, ** $p < 0.01$, *** $p < 0.001$ (two-tailed t-test), as compared to 0H. (c) Phospho-p38 and p38 α expression in liver of CTR mice before (0H) and after (24H to 72H) CCl₄ exposure. HSC70 served as a loading control. Lanes showed samples from independent biological replicates and were noncontiguous (black line). The displayed figure was cropped and the original images are part of the Supplementary Data. (d) Densitometry analysis of P-p38 vs p38 α protein levels before (0H) and after (24H to 72H) CCl₄ injection. Data represent the mean \pm SEM ($n \geq 3$ per group). * $p < 0.05$, ** $p < 0.01$, *** $p < 0.001$ (two-tailed t-test) as compared to 0H.

thioacetamide (TAA) and DiEthyl-Nitrosamine (DEN)-induced HCC mice models revealed that p38 α acts as a tumor suppressor by curtailing ROS accumulation protecting against cell death, subsequent compensatory hepatocyte proliferation and liver tumor development^{23–25}. Collectively, these studies highlight that p38 α displays several functions that critically depend on the physiopathological context. However, the impact of p38 α deletion during acute liver injury in completely mature adult hepatocytes is still an open question.

In that context, to determine the role of p38 α in the adult liver, we developed a mice model allowing the deletion of p38 α in mature hepatocytes. Using acute liver injury model, our findings reveal quite unexpectedly that p38 α deletion is translated into a potent hepatoprotective response against liver injury. Interestingly, we demonstrated that p38 α deficiency instructs the inflammatory response to promote efficient tissue repair.

Results

p38 α deletion protects mice against acute hepatocellular damage. Acute administration of carbon tetrachloride (CCl₄), is widely used in experimental animal models of liver failure that mimics human hepatic response against toxic compounds^{26,27}. CCl₄ is a strong hepatotoxin that induces overproduction of ROS, lipid peroxidation of membranes, causes hepatocyte death and inflammation, resulting to severe hepatotoxicity^{28,29}. Protection against apoptosis, inflammation and oxidative stress associated with a pro-regenerative response of the hepatocytes are crucial to ensure efficient tissue repair after detrimental CCl₄ exposure. First, to evaluate the activity of p38 α during acute liver injury, control mice were injected by a single dose of CCl₄ and liver and sera were collected during time course kinetic (Fig. 1a). A single-dose of CCl₄ induced significant liver injuries reflected by hepatocyte cytolysis that we monitored by the evaluation of ALT (Alanine Transaminase) plasma level (Fig. 1b). Indeed, ALT level picked from 24 and 48 hours (injury phase) post-injection of CCl₄ and gradually decreased at 60 and 72 hours (recovery phase) (Fig. 1b). In that context, we investigated the profile of p38 α phosphorylation/activation in the injured liver. To that end, p38 α and Thr180/Tyr182 phospho-p38 protein levels were measured by western blot analysis in a time course experiment (Fig. 1c,d). We first observed that the expression of p38 α was stable all along the kinetic (Fig. 1c). Second, whereas in the resting liver (0H) we detected a weaker signal of P-p38, the phosphorylation of p38 increased gradually after CCl₄ exposure, concomitant with the increasing tissue injury observed in the liver (Figs 1b and 2b,c) and reached a plateau at 40 hours until the end of the kinetic (Fig. 1c,d). These findings indicated that acute liver injury mediated by CCl₄ exposure induced specific activation of p38 α .

To better characterize the role of p38 α during CCl₄ injury, hepatocyte-specific deletion of p38 α (p38 $\alpha^{\Delta H}$) was achieved by crossing mice carrying conditional loxP-flanked p38 α alleles (p38 $\alpha^{fl/fl30}$) with transgenic mice expressing the Cre recombinase under the control of the hepatospecific transthyretin promoter (TTR-Cre

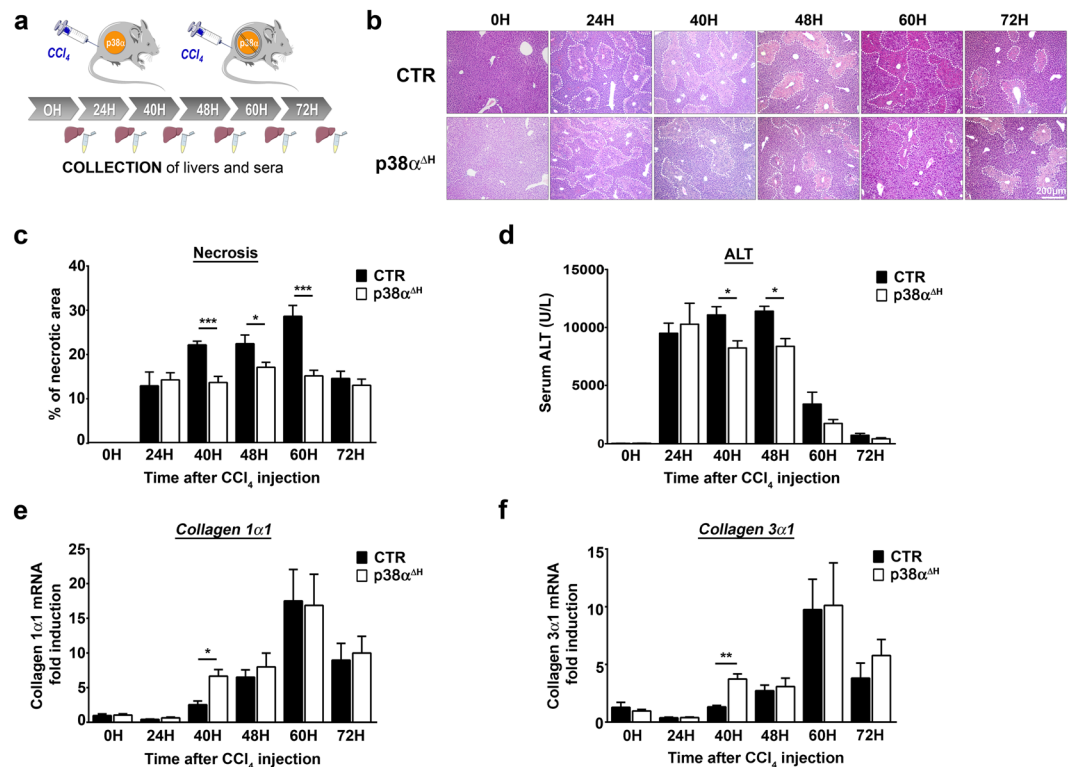


Figure 2. p38 α ablation in mature hepatocyte is hepatoprotective against CCl₄-induced liver injury. **(a)** Schematic representation of experimental procedure for CCl₄ injection in control mice (CTR) and p38 $\alpha^{\Delta H}$ mice. **(b)** Representative haematoxylin and eosin (H&E) staining of liver tissue sections from CTR and p38 $\alpha^{\Delta H}$ mice at different time points after CCl₄ injection. **(c)** Quantification of necrotic area from H&E stained CTR and p38 $\alpha^{\Delta H}$ liver sections at indicated time points after CCl₄ injection. Data represent the mean \pm SEM ($n \geq 7$ per group); * $p < 0.05$, *** $p < 0.001$ (two-tailed t-test). Average alanine aminotransferase (ALT) levels in CTR and p38 $\alpha^{\Delta H}$ sera samples at indicated time points after CCl₄ injection. Data represent the mean \pm SEM ($n \geq 6$ per group); * $p < 0.05$ (two-tailed t-test). **(e,f)** Relative mRNA level of *Collagen 1 α 1* **(e)** and *Collagen 3 α 1* **(f)** measured by quantitative PCR in CTR and p38 $\alpha^{\Delta H}$ liver samples at indicated time points after CCl₄ injection. Gene expression levels were normalized to the abundance of *18s* mRNA for each sample. Data represent the mean \pm SEM ($n \geq 6$ per group); * $p < 0.05$, ** $p < 0.01$ (two-tailed t-test).

Tam³¹); Tamoxifen diet induces very efficient ablation of p38 α expression in the liver of p38 $\alpha^{\Delta H}$ mice even though some remaining expression of p38 α was visible due to the presence of nonparenchymal cells that are not targeted by the TTR-Cre transgene (Supplementary Fig. 1a). Interestingly, following p38 α hepatospecific deletion (p38 $\alpha^{\Delta H}$) and under steady state conditions, we did not observe any signs of alterations within liver parenchyma. From these results, we concluded that p38 α expression in adult hepatocyte is not absolutely required to maintain liver homeostasis during steady-state conditions.

p38 $\alpha^{\Delta H}$ mice and their respective controls were challenged by a single CCl₄ injection and we monitored in time the hepatocyte cytolysis and liver damage (Fig. 2a). H&E staining of liver sections indicate that significant necrosis was already present from 24 hours in the liver of p38 $\alpha^{\Delta H}$ and control mice (Fig. 2b,c, Supplementary Fig. 1b). Interestingly, necrotic areas increased gradually and peaked at 60 hours post-CCl₄, to diminish at 72 hours in the liver of control mice (Fig. 2b,c). However, although necrotic areas were still evident between 40 and 48 hours in the liver of p38 $\alpha^{\Delta H}$ mice, the intensity of necrosis was markedly reduced as compared to the controls (Fig. 2b,c). Accordingly, ALT levels in p38 $\alpha^{\Delta H}$ mice remained strictly lower compared to control mice at these time points (Fig. 2d). Furthermore, cleaved caspase-3 staining was used to examine apoptosis of hepatocytes in both group of mice at 24, 40 and 48 hours post-CCl₄ treatment (Supplementary Fig. 1c). Our observations revealed that apoptotic response consecutive to CCl₄ challenge was not impaired in p38 $\alpha^{\Delta H}$ liver and could not account for the decrease of both necrotic areas and ALT levels observed in p38 α -related deficiency context (Supplementary Fig. 1c,d). To rule out the possibility that differential CCl₄ bioactivation could be responsible for the variation in the liver injury between control and p38 $\alpha^{\Delta H}$ mice, we measured mRNA level of *cyp2e1*, a major CCl₄-metabolizing enzyme. First, we did not find difference in the mRNA level of *cyp2e1* under steady state conditions between both groups of mice (Supplementary Fig. 1e). Moreover, consistent with previous reports^{32,33}, the CCl₄ treatment resulted in a decrease of *cyp2e1* mRNA level between 12 and 24 hours, indicating the same metabolism process of CCl₄ compound in both groups of mice (Supplementary Fig. 1e). Interestingly, we monitored collagens 1 α 1 (Fig. 2e) and 3 α 1 (Fig. 2f) mRNA levels and we found an up-regulation at 40 hours in the liver of p38 $\alpha^{\Delta H}$ mice as compared to control one (Fig. 2e,f), reflecting an earlier tissue repair response under

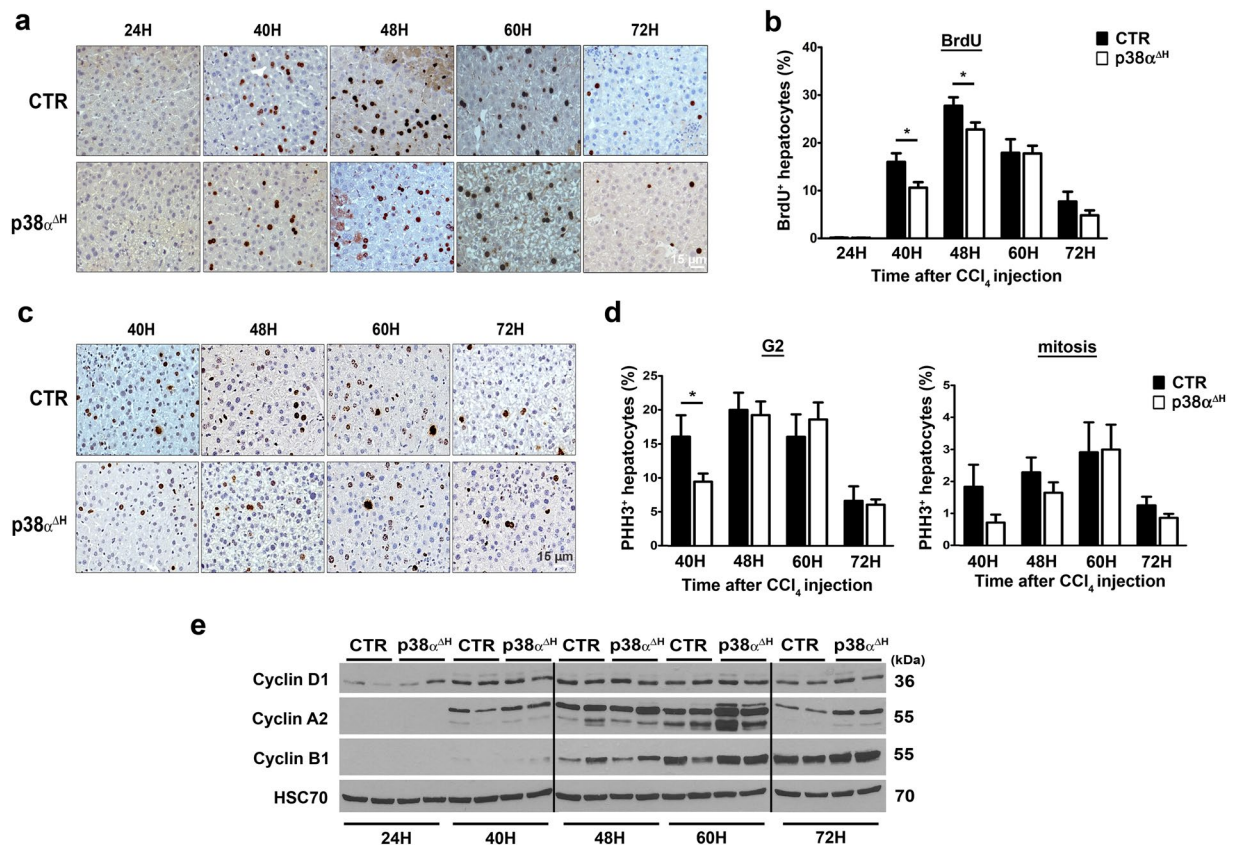


Figure 3. p38 α deficiency does not favor hepatocyte proliferation during acute injury. (a) Representative BrdU immunohistochemistry of control (CTR) and p38 $\alpha^{\Delta H}$ liver tissue at indicated time points after CCl₄ injection. (b) Quantitative analysis of BrdU labeled CTR and p38 $\alpha^{\Delta H}$ liver sections (percentage of BrdU⁺ hepatocytes). Data represent the mean \pm SEM ($n \geq 6$ per group); * $p < 0.05$ (two-tailed t-test). (c) Representative Phospho-Histone H3 (PHH3) immunohistochemistry of CTR and p38 $\alpha^{\Delta H}$ liver tissue at indicated time points after CCl₄ injection. (d) Quantitative analysis of PHH3⁺ hepatocytes in G2 phase (left panel) and mitosis (right panel) in CTR and p38 $\alpha^{\Delta H}$ livers (histologic distinction of PHH3⁺ hepatocytes). Data represent the mean \pm SEM ($n \geq 6$ per group). * $p < 0.05$ (two-tailed t-test). (e) Immunoblot of proteins regulating cell cycle progression (Cyclin D1, A2 and B1) in CTR and p38 $\alpha^{\Delta H}$ liver samples at indicated time points after CCl₄ injection. Two representative samples are shown for each analyzed point. HSC70 served as a loading control. Lanes were noncontiguous (black line). The displayed figure was cropped and the original images are part of the Supplementary Data.

p38 α deficiency. These findings suggest that p38 α ablation in adult hepatocytes both buffers liver injury and favors a better response in tissue recovery.

Proliferative response induced by acute CCl₄ was not affected by p38 α ablation. Since p38 α MAPK has been largely reported as a negative regulator of cellular proliferation controlling the induction of both G1/S and G2/M cell cycle checkpoints^{34–37}, we checked the consequences of p38 α deficiency on hepatocyte proliferative response after CCl₄ exposure. We monitored bromodeoxyuridine (BrdU) incorporation (Fig. 3a) in both control and p38 $\alpha^{\Delta H}$ livers during time-course kinetic. BrdU-positive hepatocytes were detected as soon as 40 hours post-CCl₄ and the percentage of BrdU-positive hepatocytes peaked at 48 hours, to gradually decrease afterward, in both mice groups (Fig. 3b). Contrary to what we expected, we did not observe a global enrichment of BrdU-positive hepatocytes in p38 $\alpha^{\Delta H}$ livers. In fact, BrdU immune-reactive cells were modestly decreased in p38 $\alpha^{\Delta H}$ livers compared to control livers at 40 and 48 hours post-CCl₄ exposure (Fig. 3b). To reinforce these interesting results, we analyzed G2 phase and mitosis progression using PHH3 labeling (Fig. 3c,d). In lines with the assessment of BrdU analysis in p38 $\alpha^{\Delta H}$ livers, the percentage of PHH3-positive hepatocytes was slightly reduced at 40 hours after CCl₄ exposure compared to control livers (Fig. 3d). Moreover, molecular analysis of key drivers of cell cycle progression (cyclin D1 (G1 phase), A2 (S phase) and B1 (G2/M)), did not reveal significant differences between the two groups of mice (Fig. 3e). Altogether, these data revealed that p38 α deficiency does not impact on hepatocyte cell cycle during acute injury. Importantly, our findings revealed that the hepatoprotective response driven by p38 α deletion is largely independent of its known role of cell cycle checkpoint.

Enhancement of antioxidative response protect against CCl₄-mediated injury in the absence of p38 α . Since CCl₄ causes severe liver cell damages through a strong elevation of oxidative stress response^{38,39}

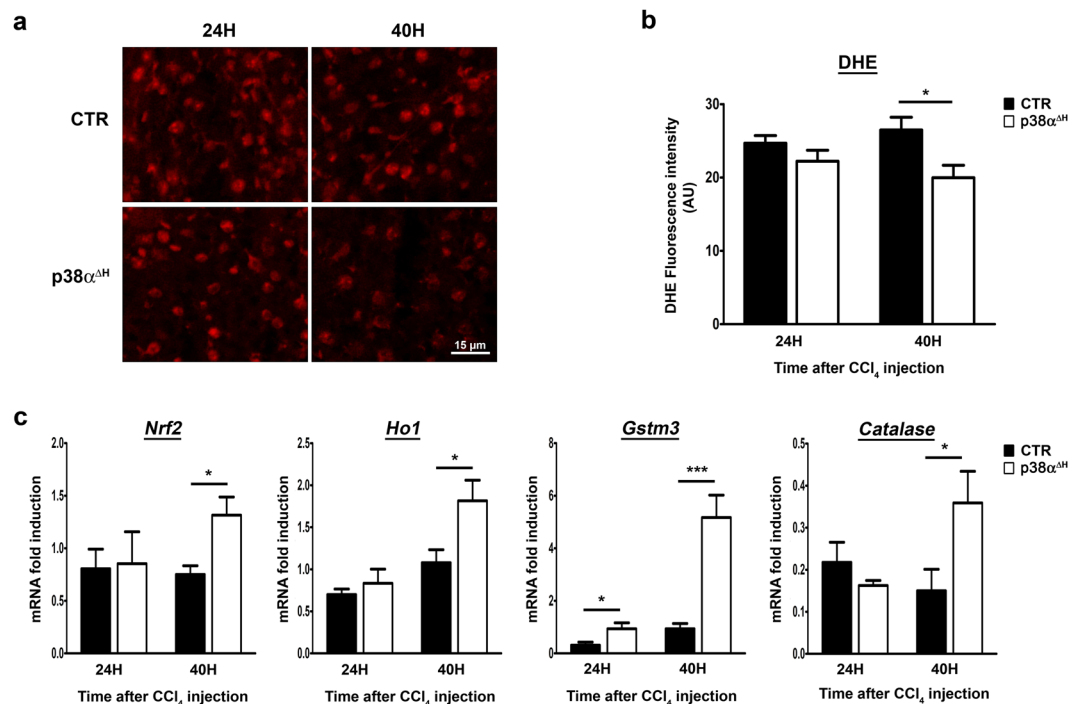


Figure 4. Enhancement of the anti-oxidant response in the liver of p38 $\alpha^{\Delta H}$ mice after acute CCl₄ exposure. (a) Representative images of Dihydroethidium (DHE) staining of control (CTR) and p38 $\alpha^{\Delta H}$ liver sections at 24 and 40 hours post-CCl₄. (b) Quantification of DHE fluorescence intensity (arbitrary unit) obtained from staining of CTR and p38 $\alpha^{\Delta H}$ liver sections at 24 and 40 hours post-CCl₄. Data represent the mean \pm SEM ($n \geq 5$ per group). * $p < 0.05$ (two-tailed t-test). (c) Relative mRNA level of antioxidant genes (*Nrf2*, *Ho1*, *Gstm3* and *Catalase*) measured by quantitative PCR in CTR and p38 $\alpha^{\Delta H}$ liver samples at 24 and 40 hours post-CCl₄. Gene expression levels were normalized to the abundance of *18s* mRNA for each sample. Data represent the mean \pm SEM ($n \geq 6$ per group). * $p < 0.05$, *** $p < 0.001$ (two-tailed t-test).

and that p38 α is a mediator of the cellular redox balance in hepatocytes^{24,25,40}, we tested whether the hepatoprotective effect observed after p38 α ablation could be attributable to an enhancement of the antioxidative response.

The general level of hepatic ROS was assessed by the fluorescent dye dihydroethidine (DHE) on fresh frozen liver sections from both control and p38 $\alpha^{\Delta H}$ mice (Fig. 4a,b). Whereas no significant differences in ROS levels were observed at 24 hours post-CCl₄ in the liver of both p38 $\alpha^{\Delta H}$ and control mice, we did notice, at 40 hours, that ROS accumulation was largely decreased in p38 $\alpha^{\Delta H}$ livers (Fig. 4a,b). This observation indicated that p38 α deficiency dampened oxidative stress. To gain insights into the signaling pathway, we investigated the Nrf2-mediated signaling as an essential component for the inhibition of oxidative stress in mice during acute liver injury^{41–43}. Interestingly, we found that Nrf2 transcripts (Fig. 4c) and its downstream effectors Ho-1, Catalase and Gstm3 (Fig. 4c) were significantly enhanced in p38 $\alpha^{\Delta H}$ compared to control livers at 40 hours post-CCl₄ injury. These findings suggested that p38 α deficiency is translated into a protective effect against CCl₄-induced ROS formation at least through Nrf2 pathway.

p38 α deletion impacts on the inflammatory response during acute liver injury. Interestingly, at the level of H&E staining, we observed along the kinetic read-out, a substantial increase of inflammatory cells within necrotic areas in p38 $\alpha^{\Delta H}$ compared to control livers (Fig. 5a). We then extracted immune cells from the livers and confirmed their increase in p38 $\alpha^{\Delta H}$ mice compared to control mice at 40 hours after CCl₄ injury (Fig. 5b). Interestingly, at 60 hours, the number of immune cells decreased in p38 $\alpha^{\Delta H}$ liver but still remained higher than in control liver (Fig. 5b). To go further, we monitored chemotactic signals, which play an essential role during acute liver injury by managing the migration of immune cells⁴⁴. We found a significant up-regulation of both Ccl2 (Fig. 5c) and Ccl5 (Fig. 5d) at 40 hours post-CCl₄ challenge, suggesting that these chemokines favor the drastic immune cell recruitment in p38 $\alpha^{\Delta H}$ livers.

Next, we evaluated common genes involved in inflammation on whole liver tissue from both groups of mice. Importantly, at 40 hours post-injury, we found a concomitant up-regulation of *Tnf α* (Fig. 5e) and *Tgf β* (Fig. 5f) expression without modifications in *Il1 β* mRNA level (Fig. 5g) suggesting a particular inflammatory flavor sustaining tissue repair. Altogether, our data suggested that the increase in immune cells could be involved into the hepatoprotective response driven by p38 α ablation.

To finally prove that the recruitment of the immune cells mediated the hepatoprotective response driven by p38 α deletion, we blocked Ccl2/Ccl5 signals using specific neutralizing antibodies 5 hours before CCl₄ exposure (Fig. 6a). We validated the effect of antibodies blockade by counting immune populations extracted from the

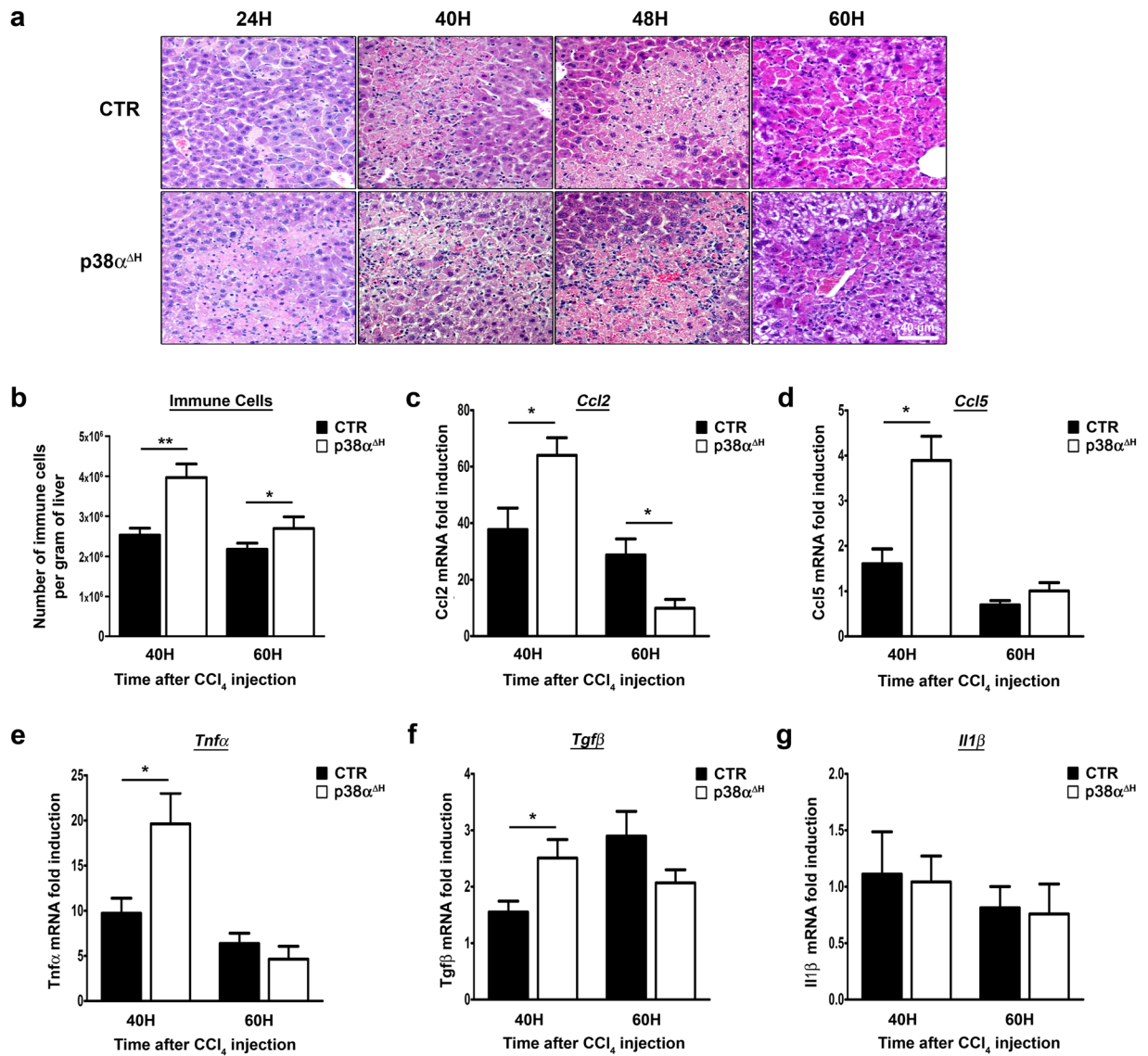


Figure 5. p38 α deficiency instructs the inflammatory response to promote efficient tissue repair. (a) Representative photomicrographs of immune infiltration with H&E staining in control (CTR) and p38 $\alpha^{\Delta H}$ liver sections at different time points after CCl₄ injection. (b) Number of hepatic immune cells per gram of liver in CTR and p38 $\alpha^{\Delta H}$ mice at 40 and 60 hours post-CCl₄. Data represent the mean \pm SEM ($n \geq 5$ per group). * $p < 0.05$, ** $p < 0.01$ (two-tailed t-test). (c–g) Relative mRNA level of *Ccl2*, *Ccl5*, *Tnf α* , *Tgf β* and *Il1 β* measured by quantitative PCR in CTR and p38 $\alpha^{\Delta H}$ liver samples at indicated time points after CCl₄ injection. Gene expression levels were normalized to the abundance of *18s* mRNA for each sample. Data represent the mean \pm SEM ($n \geq 5$ per group). * $p < 0.05$ (two-tailed t-test).

livers and found a drastic decrease in the total number of immune cells (Fig. 6b) in both groups of mice. In the meantime, we showed that antibody blockade provoked a dramatic abolishment of hepatoprotection in p38 $\alpha^{\Delta H}$ livers through an amplification of necrotic regions (Fig. 6c) associated with a reduced anti-oxidative response (Fig. 6d). Moreover, we also found an accentuation of liver injury in control mice (Fig. 6c), suggesting that these hepatoprotective immune cells were already present in p38-proficient livers (Fig. 6b) but were massively recruited under p38 α deficiency. Interestingly, we found a clear reduction in the level of *Tnf α* and *Tgf β* transcripts (Fig. 6e) in both groups of mice concomitantly upregulated at 40 hours post-CCl₄ challenge after *Ccl2/Ccl5* blockade (Fig. 6e,f). These findings indicated that the combination of these two signaling (*Tnf α* and *Tgf β*) participate to the hepatoprotective response. Accordingly, downregulation of *Collagen 1 α 1* level was also observed after *Ccl2/Ccl5* blockade (Fig. 6f), confirming the attenuation of liver tissue repair.

Altogether, our data clearly demonstrated the crucial requirement of these two chemotactic signals favoring the recruitment of immune cells to mediate the hepatoprotective response driven by p38 α ablation.

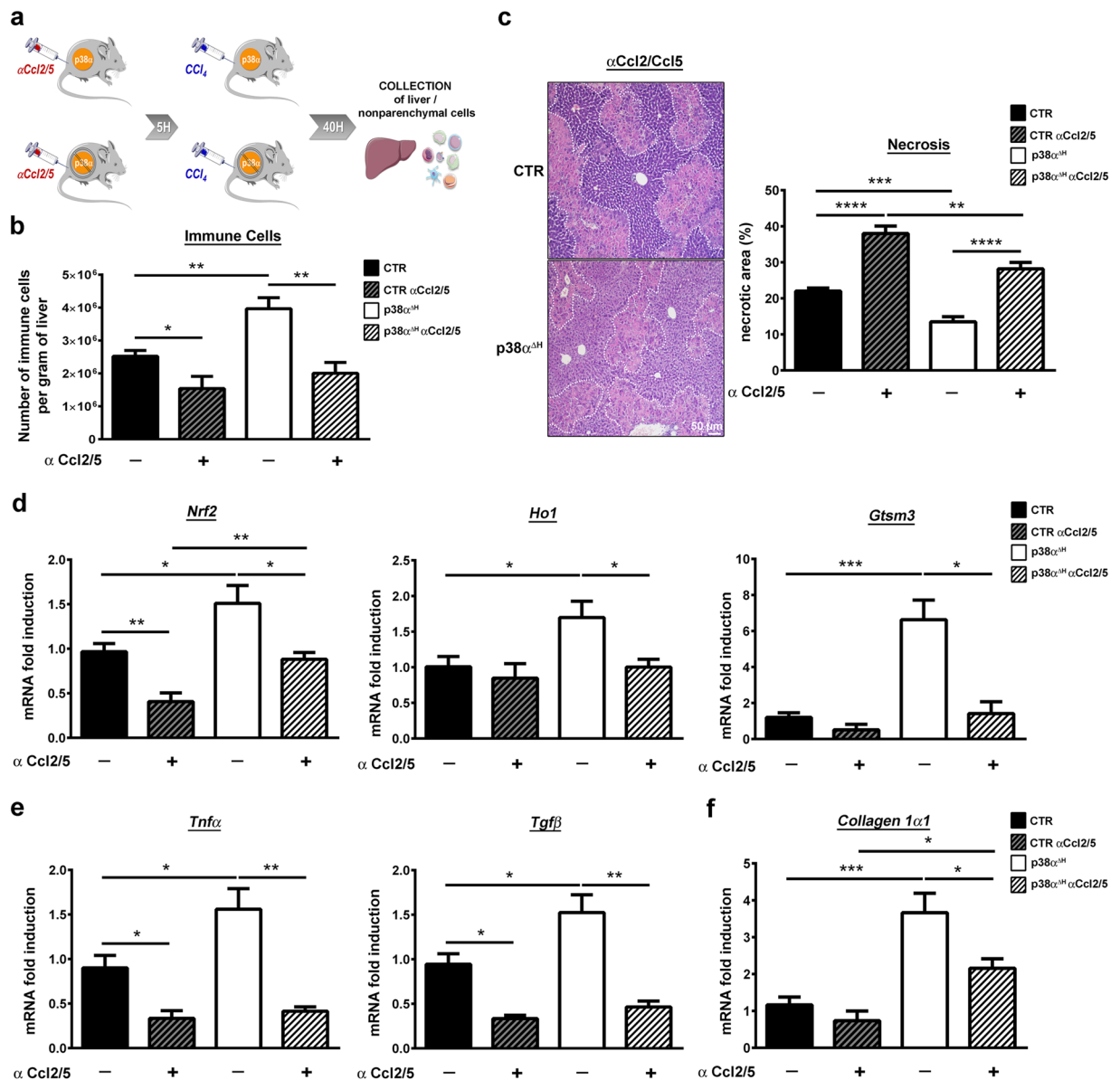


Figure 6. Blockade of Ccl2/Ccl5 chemotactic signals impairs hepatoprotective effect coupled to p38 α deficiency during acute liver injury. **(a)** Schematic representation of experimental procedure for Ccl2 and Ccl5 blockade. Control (CTR) and p38 $\alpha^{\Delta H}$ mice were sacrificed at 40 hours after CCl₄ injection. **(b)** Number of immune cells per gram of liver in CTR and p38 $\alpha^{\Delta H}$ mice treated or not by Ccl2/Ccl5 antibodies, 40 hours after CCl₄ exposure. Data represent the mean \pm SEM ($n \geq 5$ per group). * $p < 0.05$, ** $p < 0.01$ (two-tailed t-test). **(c)** Necrotic area analysis by liver section H&E staining of CTR and p38 $\alpha^{\Delta H}$ mice treated or not by Ccl2/Ccl5 antibodies and its quantification at 40 hours post-CCl₄. Data represent the mean \pm SEM ($n \geq 5$ per group). ** $p < 0.01$, *** $p < 0.001$, **** $p < 0.0001$ (two-tailed t-test). **(d)** Relative mRNA level of antioxidant genes (*Nrf2*, *Ho1* and *Gstm3*) measured by quantitative PCR in CTR and p38 $\alpha^{\Delta H}$ livers issued from mice treated or not by Ccl2/Ccl5 antibodies and its quantification at 40 hours post-CCl₄. Gene expression levels were normalized to the abundance of *18s* mRNA for each sample. Data represent the mean \pm SEM ($n \geq 3$ per group). * $p < 0.05$, ** $p < 0.01$, *** $p < 0.001$ (two-tailed t-test). **(e, f)** Relative mRNA level of *Tnf α* and *Tgf β* (E) and *Collagen 1 α 1* (F) measured by quantitative PCR in CTR and p38 $\alpha^{\Delta H}$ livers issued from mice treated or not by Ccl2/Ccl5 antibodies and its quantification at 40 hours post-CCl₄. Gene expression levels were normalized to the abundance of *18s* mRNA for each sample. Data represent the mean \pm SEM ($n \geq 3$ per group). * $p < 0.05$, ** $p < 0.01$, *** $p < 0.001$ (two-tailed t-test).

Discussion

Drug-induced liver injury and acute liver failure (ALF) remains a major problem in Western societies^{45,46}. While significant progress has been made in the understanding of intracellular signaling mechanisms of toxicity related to various compounds in hepatocytes, e.g. paracetamol⁴⁷, there is still an urgent need to develop potent

therapeutic strategies to circumvent ALI and ALF. ALI can be studied in animal models and in isolated hepatocytes and most mechanisms are translatable to humans^{27,48}. Due to its strong ability to integrate a variety of signaling pathways, previous reports highlighted p38 Mitogen Activated Protein Kinases (MAPKs) as potential appealing targets to improve ALI outcome. Most of these studies were done by using a hepatospecific ablation of p38 α isoform arising either during foetal (hepatoblasts) or neonatal (immature hepatocytes) development. As p38 α plays a crucial role in cellular differentiation^{18,49,50}, we supposed that earlier deletion could impair differentiation of hepatocytes and terminal liver maturation. In the present study, we developed a new inducible and hepatospecific mice model in which p38 α isoform was completely deleted in mature hepatocytes. Until now, p38 α ablation in the liver was shown as deleterious in different models of liver injury^{22,25,51}. In this study, using the CCl₄ model of acute liver injury, we demonstrate for the first time that p38 α deletion generated a pro-hepatoprotective response against liver injury. Remarkably, we showed that p38 α deficiency after CCl₄ exposure, shaped the inflammatory response to promote efficient tissue repair. Finally, we evidenced that hepatoprotective response driven by p38 α ablation was critically dependent on Ccl2/Ccl5 chemotactic signals, as their blockade dramatically exacerbated liver injury.

Following injuries, p38 α MAPK displayed a wide range of cellular responses to ensure the maintenance of tissue homeostasis. Due to its major role as a negative regulator of cellular proliferation^{20,21,36}, we expected to observe an extensive enhancement of hepatocytes proliferation secondary to p38 α ablation. Differently, we found a lower proliferative response, reflecting buffered injuries (concomitant decrease in necrotic areas and ALT levels) in p38 $\alpha^{\Delta H}$ liver as compared to control one. Importantly, our data showed that p38 α ablation did not increase the proliferation of hepatocytes after CCl₄ exposure and also revealed that the function of p38 α as a cell cycle checkpoint does not account for the hepatoprotective effect. Our findings are quite novel, since increased proliferation has been until now considered a hallmark of p38 α deficient cells²³.

Interestingly, we demonstrated that the deletion of p38 α isoform in adult hepatocytes has strong repercussions on the immune microenvironment to mediate a potent hepatoprotective response favoring efficient hepatic tissue repair. Indeed, we found a drastic infiltration of immune cells mediated by Ccl2/Ccl5 chemokines. In addition, we clearly identified that Ccl2/Ccl5 chemotactic signals were crucial in that response as their neutralization sensitized to increase liver injury. Therefore, our findings highlight a new aspect in the pleiotropic role of p38 α in hepatocytes during acute liver injury, as until now the beneficial effect of p38 α deletion was strictly observed when performed in immune effectors such as liver myeloid cells or T/NKT cells^{51,52}. Furthermore, the work of Kang and collaborators provided evidence that p38 α ablation in hepatocytes was fueled by a drastic accentuation of liver injury associated with a massive inflammatory cell recruitment⁵¹. This study was conducted using a different model of acute liver injury (e.g. ConA). Collectively, these data underlie that the nature of stimuli-induced injury greatly influences the cellular response of p38 α , as it does not trigger the same immune effectors involving preferentially either myeloid cells (e.g. CCl₄, APAP) or lymphoid T cell reservoir (ConA)⁵³. Therefore, it turns out that depending on the initial stimuli, the flavor of the inflammatory response dictates the outcome of tissue response. Our work clearly strengthens the critical connection between hepatocyte and immune system during acute liver injury and calls into question about the nature of the effectors involved in hepatoprotection. Further experiments are required to elucidate the molecular support of this dialogue. It is noteworthy that we found that the antioxidative response was determinant in the mediation of hepatoprotection in p38 $\alpha^{\Delta H}$ liver. Interestingly, Ccl2/Ccl5 antibody blockade considerably diminished this antioxidative response in our model. These observations are of importance as they illustrated that immune system could behave also as an additional partner to adapt the redox balance during liver injury⁵⁴.

Finally, due to very limited therapeutic options for the treatment of acute liver injury, our work provides another field of treatment targeting specifically p38 α in hepatocyte and manipulating immune response.

Materials and Methods

Generation of conditional knockout mice and animal care. Mice carrying two loxP sites flanking (floxed) exons 2 and 3 of the p38 α gene (p38 $\alpha^{fl/fl}$)³⁰ were interbred with TTR-Cre-Tam mice expressing a tamoxifen-inducible Cre recombinase under the control of the hepatocyte-specific transthyretin promoter³¹ to generate p38 $\alpha^{\Delta H}$ mice (p38 $\alpha^{fl/fl}$ TTR-Cre⁺-Tam) on the C57Bl6J genetic background. In all experiments, littermate carrying the respective loxP-flanked alleles but lacking expression of the Cre recombinase were used as controls (p38 $\alpha^{fl/fl}$ TTR-Cre⁻-Tam). Mice were maintained at a constant temperature and humidity in light-controlled room with a 12 hours light cycle. They had free access to food (SAFE Laboratory) and tap water. To induce specific hepatocyte p38 α deletion, four weeks old male p38 $\alpha^{\Delta H}$ were fed with tamoxifen diet (+1000 mg/kg TAM A115-T7100, Ssniff, Germany) during five days as well as their control littermates (p38 $\alpha^{fl/fl}$ TTR-Cre⁻-Tam). All experiments were conducted in accordance with the institutional guidelines and the recommendations for the care and use of laboratory animals put forward by the Directive 2010/63/EU. This revises Directive 86/609/EEC on the protection of animals used for scientific purposes. All animal studies were approved by the Ministère de l'Enseignement Supérieur, de la Recherche et de l'Innovation (MESRI) and the Direction Départementale des Services Vétérinaires de Paris (agreement No. 75–956) and by the Mouse Facility Core laboratories (Institut Cochin, Inserm U1016/ CRC UMRS1138).

Acute liver injury model. Experiments were performed both on control (p38 $\alpha^{fl/fl}$ TTR-Cre⁻-Tam) and p38 $\alpha^{\Delta H}$ (p38 $\alpha^{fl/fl}$ TTR-Cre⁺-Tam) male mice between 8 and 10 weeks of age. CCl₄ (Merck, Germany) dissolved with sunflower oil [1:9] was administered intraperitoneally (IP) at 0.56 g/kg of body weight. Two hours before tissue harvest, mice were intraperitoneally injected with 50 mg/kg of Bromodeoxyuridine (BrdU) (Merck, Germany). Mice were euthanized at 0, 12, 24, 40, 48, 60 and 72 hours post-CCl₄. After sacrifice, part of liver tissue was fixed in 4% neutral buffered formalin for immunohistochemistry analysis. The remaining liver tissue was flash frozen in liquid nitrogen and stored at –80 °C until used.

Gene	Forward	Reverse
18S	GTA-ACC-CGT-TGA-ACC-CCA-TT	CCA-TCC-AAT-CGG-TAG-TAG-CG
Catalase	ACA-TGG-TCT-GGG-ACT-TCT-GG	CAA-GTT-TTT-GAT-GCC-CTG-GT
Ccl2	TCT-GGG-CCT-GCT-GTT-CAC-A	GGA-TCA-TCT-TGC-TGG-TGA-ATG-A
Ccl5	GCT-GCT-TTG-CCT-ACC-TCT-CC	TCG-AGT-GAC-AAA-CAC-GAC-TGC
Collagen 1 α 1	GAG-CGG-AGA-GTA-CTG-GAT-CG	GCT-TCT-TTT-CCT-TGG-GGT-TC
Collagen 3 α 1	GAA-GTC-TCT-GAA-GCT-GAT-GGG	TTG-CCT-TGC-GTG-TTT-GAT-ATT-C
Cyp2e1	CGT-TGC-CTT-GCT-TGT-CTG-GA	AAG-AAA-GGA-ATT-GGG-AAA-GGT-CC
Gstm3	TAT-GAC-ACT-GGG-CTA-TTG-GAA-CAC	GGG-CAT-CCC-CCA-TGA-CA
Ho1	AAG-CCC-AGA-ATG-CTG-AGT-TC	GCC-GTG-TAA-TAT-GGT-ACA-AGG-A
IL1 β	GCC-CAT-CCT-CTG-TGA-CTC-AT	AGG-CCA-CAG-GTA-TTT-TGT-CG
Nrf2	AGG-ACA-TGG-AGC-AAG-TTT-GG	TCT-GTC-AGT-GTG-GCT-TCT-GG
Tgfb β 1	TGG-CGT-TAC-CTT-GGT-AAC-C	GGT-GCT-GGG-CCC-TTT-CCA-G
Tnf α	CAT-CTT-CTC-AAA-ATT-CGA-GTG-ACA-A	TGG-GAG-TAG-ACA-AGG-TAC-ACC-CC

Table 1. Primer Sequences.

Antibody depletion experiment. Five hours before CCl₄ treatment, mice received a single IP injection of a cocktail of anti-Ccl2 (clone 2H5, Bio X Cell) antibody at a dose of 7.5 mg/kg and anti-Ccl5 antibody (clone 53405, R&D systems) at a dose of 1.0 mg/kg or control antibody (Polyclonal Armenian Hamster IgG, Bio X Cell; Normal Rat IgG control, R&D Systems). The efficacy of antibody depletion was evaluated 40 hours after CCl₄ treatment.

Serum Transaminase activity. Blood was collected from intracardiac puncture on anesthetized mice during time-course kinetic after CCl₄ treatment and the activity of serum alanine aminotransferase [ALT] was measured using the AU400 chemistry analyzer (Olympus) (Biochemistry Facility, CRI Institute, Paris, France).

Nonparenchymal cell isolation. As previously described⁵⁵, livers were harvested and perfused with Hank's balanced salt solution (1X HBSS) containing 10 mM HEPES, to remove circulating blood cells. The liver was passed through a stainless steel mesh in RPMI 1640 supplemented with 2% heat-inactivated fetal calf serum (FCS) (Gibco, ThermoFisher Scientific), 5 mM HEPES, 2 mM Glutamax (Gibco, ThermoFisher Scientific), 100 U/mL penicillin, 100 μ g/mL streptomycin, and 5×10^{-5} M β -mercaptoethanol (Gibco, ThermoFisher Scientific). The liver cell suspension was collected and parenchymal cells were separated from nonparenchymal cells (NPCs) by centrifugation for 3 min at 800 rpm. The supernatant containing the NPCs was collected and centrifuged for 10 min at 1500 rpm. The pellet was then resuspended in 35% Percoll (GE Healthcare) diluted in RPMI 1640 supplemented with 2% FCS, 20 min at room temperature, at 2,000 rpm. The NPC fraction was collected at the bottom and the cells were collected by two rounds of centrifugation in ice-cold PBS. Red blood cells were removed by incubation with lysis buffer ACK (0.15 M NH₄Cl, 10 mM KHCO₃ and 0.1 mM Na₂EDTA, pH 7.2). Cells were then washed in RPMI 1640 containing 10% FCS and centrifuged for 10 min at 1,500 rpm. Cells were resuspended in serum-containing medium and viable NPCs were counted by a trypan blue exclusion method, and stored on ice until further use.

Gene expression analysis. Total RNA from mouse liver tissue was extracted using Trizol (ThermoFisher Scientific). Purified RNA was then reverse-transcribed with the High-Capacity cDNA Reverse Transcription Kit (Applied Biosystems). Quantitative PCR (q-PCR) was performed using a SYBR Luminaris Color HiGreen qPCR master mix (ThermoFisher Scientific) and specific primers (see Table 1). The reactions were performed in 96-well plates in a LightCycler 480 instrument (Roche) with 40 cycles. We determined the relative amounts of the mRNAs studied by means of the second-derivative maximum method, with LightCycler 480 analysis software and 18 s mRNA as the invariant control for all studies.

Western blotting analysis. Total proteins were extracted from snap-frozen livers as described previously⁵⁶. Protein concentration was determined using the bicinchoninic acid assay (Bio-Rad Protein Assay). Proteins (40 μ g) were resolved by SDS-PAGE and then transferred onto nitrocellulose membranes (0.45- μ m pore size), which were incubated overnight at 4 °C with primary antibodies. Primary antibodies used for western blotting are referenced in Table 2. The proteinbound primary antibodies were detected with an appropriate horseradish peroxidase-conjugated secondary antibody (ThermoFisher Scientific). Immunoreactive bands were revealed using the "Clarity Western ECL Substrate" purchased from Bio-Rad. Blots were exposed to Amersham Hyperfilm (GE Healthcare Life Sciences). In all immunoblotting, HSC70 was used to normalize the results. For protein quantification, densitometry analysis was performed using Image J 1.8.0_112. Data are presented as relative units, which represent the densitometric value for the phosphoprotein of interest that was normalized to the total levels of the same protein.

Histology, immunohistochemistry. Tissue was fixed by incubation in 4% formol overnight at 4 °C and embedded in paraffin wax. Hematoxylin/eosin staining was carried out on 5- μ m paraffin sections. For immunohistochemistry, liver sections (5 μ m) were de-paraffinized and incubated in citrate buffer at 95 °C for 20 min for antigen retrieval. Sections were treated with 3% hydrogen peroxide for 15 min at room temperature and then

Antibody	Dilution	Manufacturer and Reference
BrdU	1/400	Thermo Fisher #MA5-12502
Cleaved-Caspase 3	1/100	Cell Signaling #9664
Cyclin A2	1/2000	Abcam #32386
Cyclin B1	1/1000	Cell Signalling #4138
Cyclin D1	1/3000	Pierce MA1-39546
HSC70	1/25000	Santa Cruz #7298
p38 α	1/4000	ThermoFisher Scientific #PA5-17713
PHH3	1/500	Millipore #06-570
phospho-p38	1/4000	Cell Signalling #4511

Table 2. Antibodies used in immunohistochemistry or western blot experiments.

incubated overnight at 4°C with the primary antibodies referenced in Table 2. After three washes in PBS1X, tissue sections were incubated with biotinylated anti-mouse/rabbit or rat IgG (1/200 dilution, Vector Laboratories, CA, USA) for 1 hr at RT and then washed three times in PBS1X, after which streptavidin–horseradish peroxidase conjugates (Vector Laboratories, CA, USA) were added and the slides incubated for 45 min. After three washes with PBS1X, DAB solution (Vector Laboratories, CA, USA) was added and the slides were counterstained with haematoxylin.

In situ detection of ROS. Fresh cross sections (8 μm) of unfixed, frozen mouse livers were immediately incubated with 5 μM DHE at 37°C for 30 minutes in a humidified chamber, subsequently washed twice with ice-cold phosphate-buffered saline, and coverslipped⁵⁷. The fluorescence intensity of DHE staining was measured with ImageJ software.

Image acquisition and analysis. Concerning HE, BrdU and PHH3 labelling, images were taken using a Nikon Statif Eclipse E600 microscope with x10 and x20 magnification, 1.4–0.7 NA PL-APO objectives, a DXM1200 cooled CCD camera (Nikon), and ACT-1 (version 2.63; Universal Imaging). For cleaved-caspase 3 labelling, images were taken using an Olympus BX63F, at 4x magnification Uplan FLN objective, an Olympus DP73 camera and Metamorph software. Necrotic area were quantified by morphometric analysis using an open-source ImageJ software in 5 fields at x10 magnification. For BrdU/PHH3 staining, 4000 hepatocytes (for each liver sample analyzed) were counted; at least 10 areas of 33,500 μm^2 were analyzed. Cleaved-caspase 3 immunostaining was quantified by color segmentation using an open-source ImageJ software in 5 fields at 4x magnification. Adobe Photoshop CS (Adobe Systems Software) was used for figure construction.

Statistical analysis. Statistical significance was determined with a 2-tailed Student's t test performed using GraphPad Prism 6.0 (GraphPad Software Inc). All data are representative of 3 to 10 animals of each genotype and are expressed as mean \pm SEM. A P value of less than 0.05 was considered statistically significant.

References

- Bernal, W. & Wendon, J. Acute Liver Failure. *New England Journal of Medicine* **369**, 2525–2534 (2013).
- Björnsson, E. S., Bergmann, O. M., Björnsson, H. K., Kvaran, R. B. & Olafsson, S. Incidence, Presentation, and Outcomes in Patients With Drug-Induced Liver Injury in the General Population of Iceland. *Gastroenterology* **144**, 1419–1425.e3 (2013).
- Franco, E. Hepatitis A: Epidemiology and prevention in developing countries. *World Journal of Hepatology* **4**, 68 (2012).
- Ingawale, D. K., Mandlik, S. K. & Naik, S. R. Models of hepatotoxicity and the underlying cellular, biochemical and immunological mechanism(s): A critical discussion. *Environmental Toxicology and Pharmacology* **37**, 118–133 (2014).
- Rutherford, A. & Chung, R. Acute Liver Failure: Mechanisms of Hepatocyte Injury and Regeneration. *Seminars in Liver Disease* **28**, 167–174 (2008).
- Bantel, H. & Schulze-Osthoff, K. Mechanisms of Cell Death in Acute Liver Failure. *Frontiers in Physiology* **3** (2012).
- Diehl, A. M. Cytokine regulation of liver injury and repair. *Immunol. Rev.* **174**, 160–171 (2000).
- Jaeschke, H., Williams, C. D., Ramachandran, A. & Bajt, M. L. Acetaminophen hepatotoxicity and repair: the role of sterile inflammation and innate immunity: Acetaminophen hepatotoxicity and repair. *Liver International* **32**, 8–20 (2012).
- Kaplowitz, N. Mechanisms of liver cell injury. *J. Hepatol.* **32**, 39–47 (2000).
- Cordero-Espinoza, L. & Huch, M. The balancing act of the liver: tissue regeneration versus fibrosis. *Journal of Clinical Investigation* **128**, 85–96 (2018).
- Malhi, H. & Gores, G. J. Cellular and Molecular Mechanisms of Liver Injury. *Gastroenterology* **134**, 1641–1654 (2008).
- Chang, L. & Karin, M. Mammalian MAP kinase signalling cascades. *Nature* **410**, 37–40 (2001).
- Cuenda, A. & Rousseau, S. p38 MAP-kinases pathway regulation, function and role in human diseases. *Biochim Biophys Acta* **1773**, 1358–75 (2007).
- Nebreda, A. R. & Porras, A. p38 MAP kinases: beyond the stress response. *Trends Biochem. Sci.* **25**, 257–260 (2000).
- Raman, M., Chen, W. & Cobb, M. H. Differential regulation and properties of MAPKs. *Oncogene* **26**, 3100–3112 (2007).
- Adams, R. H. *et al.* Essential role of p38 α MAP kinase in placental but not embryonic cardiovascular development. *Mol. Cell* **6**, 109–116 (2000).
- Mudgett, J. S. *et al.* Essential role for p38 α mitogen-activated protein kinase in placental angiogenesis. *Proceedings of the National Academy of Sciences* **97**, 10454–10459 (2000).
- Tamura, K. *et al.* Requirement for p38 α in Erythropoietin Expression. *Cell* **102**, 221–231 (2000).
- Campbell, J. S., Argast, G. M., Yuen, S. Y., Hayes, B. & Fausto, N. Inactivation of p38 MAPK during liver regeneration. *The International Journal of Biochemistry & Cell Biology* **43**, 180–188 (2011).

20. Hui, L. *et al.* p38 α suppresses normal and cancer cell proliferation by antagonizing the JNK–c-Jun pathway. *Nature Genetics* **39**, 741–749 (2007).
21. Stepniak, E. c-Jun/AP-1 controls liver regeneration by repressing p53/p21 and p38 MAPK activity. *Genes & Development* **20**, 2306–2314 (2006).
22. Tormos, A. M. *et al.* Liver-specific p38 α deficiency causes reduced cell growth and cytokinesis failure during chronic biliary cirrhosis in mice. *Hepatology* **57**, 1950–1961 (2013).
23. Hui, L., Bakiri, L., Stepniak, E. & Wagner, E. F. p38 α : A Suppressor of Cell Proliferation and Tumorigenesis. *Cell Cycle* **6**, 2429–2433 (2007).
24. Sakurai, T. *et al.* p38 Inhibits Liver Fibrogenesis and Consequent Hepatocarcinogenesis by Curtailing Accumulation of Reactive Oxygen Species. *Cancer Research* **73**, 215–224 (2013).
25. Sakurai, T. *et al.* Hepatocyte Necrosis Induced by Oxidative Stress and IL-1 α Release Mediate Carcinogen-Induced Compensatory Proliferation and Liver Tumorigenesis. *Cancer Cell* **14**, 156–165 (2008).
26. Liedtke, C. *et al.* Experimental liver fibrosis research: update on animal models, legal issues and translational aspects. *Fibrogenesis & Tissue Repair* **6**, 19 (2013).
27. Maes, M., Vinken, M. & Jaeschke, H. Experimental models of hepatotoxicity related to acute liver failure. *Toxicology and Applied Pharmacology* **290**, 86–97 (2016).
28. Martínez, M., Mourelle, M. & Muriel, P. Protective effect of colchicine on acute liver damage induced by CCl₄. Role of cytochrome P-450. *J Appl Toxicol* **15**, 49–52 (1995).
29. Recknagel, R. O., Glende, E. A., Dolak, J. A. & Waller, R. L. Mechanisms of carbon tetrachloride toxicity. *Pharmacol. Ther.* **43**, 139–154 (1989).
30. Heinrichsdorff, J., Luedde, T., Perdiguero, E., Nebreda, A. R. & Pasparakis, M. p38 α MAPK inhibits JNK activation and collaborates with I κ B kinase 2 to prevent endotoxin-induced liver failure. *EMBO reports* **9**, 1048–1054 (2008).
31. Tannour-Louet, M. A tamoxifen-inducible chimeric Cre recombinase specifically effective in the fetal and adult mouse liver. *Hepatology* **35**, 1072–1081 (2002).
32. Knockaert, L. *et al.* Carbon tetrachloride-mediated lipid peroxidation induces early mitochondrial alterations in mouse liver. *Laboratory Investigation* **92**, 396–410 (2012).
33. Tierney, D. J., Haas, A. L. & Koop, D. R. Degradation of cytochrome P450 2E1: selective loss after labilization of the enzyme. *Arch. Biochem. Biophys.* **293**, 9–16 (1992).
34. Ambrosino, C. & Nebreda, A. R. Cell cycle regulation by p38 MAP kinases. *Biol Cell* **93**, 47–51 (2001).
35. Lee, K., Kenny, A. E. & Rieder, C. L. P38 Mitogen-activated Protein Kinase Activity Is Required during Mitosis for Timely Satisfaction of the Mitotic Checkpoint But Not for the Fidelity of Chromosome Segregation. *Molecular Biology of the Cell* **21**, 2150–2160 (2010).
36. Thornton, T. M. & Rincon, M. Non-classical p38 map kinase functions: cell cycle checkpoints and survival. *Int. J. Biol. Sci.* **5**, 44–51 (2009).
37. Wong, E. S. M. *et al.* p38MAPK Controls Expression of Multiple Cell Cycle Inhibitors and Islet Proliferation with Advancing Age. *Developmental Cell* **17**, 142–149 (2009).
38. Cichoż-Lach, H. Oxidative stress as a crucial factor in liver diseases. *World Journal of Gastroenterology* **20**, 8082 (2014).
39. Weber, L. W. D., Boll, M. & Stampfl, A. Hepatotoxicity and Mechanism of Action of Haloalkanes: Carbon Tetrachloride as a Toxicological Model. *Critical Reviews in Toxicology* **33**, 105–136 (2003).
40. Tormos, A. M., Taléns-Visconti, R., Nebreda, A. R. & Sastre, J. p38 MAPK: A dual role in hepatocyte proliferation through reactive oxygen species. *Free Radical Research* **47**, 905–916 (2013).
41. Cai, Z. *et al.* N-acetylcysteine protects against liver injury induced by carbon tetrachloride via activation of the Nrf2/HO-1 pathway. *Int J Clin Exp Pathol* **8**, 8655–8662 (2015).
42. Jadeja, R. N., Upadhyay, K. K., Devkar, R. V. & Khurana, S. Naturally Occurring Nrf2 Activators: Potential in Treatment of Liver Injury. *Oxidative Medicine and Cellular Longevity* **2016**, 1–13 (2016).
43. Xu, W. *et al.* The Nrf2 transcription factor protects from toxin-induced liver injury and fibrosis. *Laboratory Investigation* **88**, 1068–1078 (2008).
44. Karlmark, K. R., Wasmuth, H. E., Trautwein, C. & Tacke, F. Chemokine-directed immune cell infiltration in acute and chronic liver disease. *Expert Review of Gastroenterology & Hepatology* **2**, 233–242 (2008).
45. Bernal, W., Lee, W. M., Wendon, J., Larsen, F. S. & Williams, R. Acute liver failure: A curable disease by 2024? *Journal of Hepatology* **62**, S112–S120 (2015).
46. Lee, W. M. Drug-induced Acute Liver Failure. *Clinics in Liver Disease* **17**, 575–586 (2013).
47. Ye, H., Nelson, L. J., Moral, M. G., del, Martínez-Naves, E. & Cubero, F. J. Dissecting the molecular pathophysiology of drug-induced liver injury. *World Journal of Gastroenterology* **24**, 1373–1385 (2018).
48. Jaeschke, H., Xie, Y. & McGill, M. R. Acetaminophen-induced Liver Injury: from Animal Models to Humans. *J Clin Transl Hepatol* **2**, 153–161 (2014).
49. Segalés, J., Perdiguero, E. & Muñoz-Cánoves, P. Regulation of Muscle Stem Cell Functions: A Focus on the p38 MAPK Signaling Pathway. *Frontiers in Cell and Developmental Biology* **4** (2016).
50. Séverin, S., Ghevaert, C. & Mazharian, A. The mitogen-activated protein kinase signaling pathways: role in megakaryocyte differentiation. *Journal of Thrombosis and Haemostasis* **8**, 17–26 (2010).
51. Kang, Y. J., Bang, B.-R., Otsuka, M. & Otsu, K. Tissue-Specific Regulation of p38 α -Mediated Inflammation in Con A-Induced Acute Liver Damage. *J. Immunol.* **194**, 4759–4766 (2015).
52. Liu, J. *et al.* Deficiency of p38 α in macrophage ameliorates D-galactosamine/TNF- α -induced acute liver injury in mice. *The FEBS Journal* **284**, 4200–4215 (2017).
53. Khan, H. A., Ahmad, M. Z., Khan, J. A. & Arshad, M. I. Crosstalk of liver immune cells and cell death mechanisms in different murine models of liver injury and its clinical relevance. *HBPD INT* **16**, 245–256 (2017).
54. Li, S., Hong, M., Tan, H.-Y., Wang, N. & Feng, Y. Insights into the Role and Interdependence of Oxidative Stress and Inflammation in Liver Diseases. *Oxidative Medicine and Cellular Longevity* **2016**, 1–21 (2016).
55. L’Hermitte, A. *et al.* Lect2 controls inflammatory monocytes to constrain the growth and progression of hepatocellular carcinoma. *Hepatology*, <https://doi.org/10.1002/hep.30140> (2018).
56. Celson-Morizur, S., Merlen, G., Couton, D., Margall-Ducos, G. & Desdouets, C. The insulin/Akt pathway controls a specific cell division program that leads to generation of binucleated tetraploid liver cells in rodents. *J Clin Invest* **119**, 1880–7 (2009).
57. Gentric, G. *et al.* Oxidative stress promotes pathologic polyploidization in nonalcoholic fatty liver disease. *J Clin Invest* **125**, 981–92 (2015).

Acknowledgements

We thank Manolis Pasparakis for giving us the mice p38 α ^{fl/fl}. We thank the core facilities of the Institut Cochin, INSERM U1016 UMR CNRS 8104, Université Paris Descartes. We gratefully acknowledge the Centre d’Explorations Fonctionnelles staff for their technical assistance with mice. Centre de Recherche des Cordeliers, INSERM, Sorbonne Université, USPC, Université Paris Descartes, Université Paris Diderot, F75006 Paris, France.

This work was supported by a grant from Institut National de la Santé et de la Recherche Médicale (INSERM). M.F. was supported by a fellowship from Ecole Doctorale BioSPC, Université Paris Descartes and the Fondation pour la Recherche Médicale (FDT20170437207).

Author Contributions

M.F.: design, acquisition of all data, analysis and interpretation of all data, drafting of manuscript. M.C.: design, acquisition of data, analysis and interpretation of data (immune part of the study), critical reading of the manuscript. N.B.: performed experiments and technical support. S.P.: performed experiments (immune part of the study). R.D.: performed experiments and technical support. J.P.C.: study concept and experiments design (immune part of the study), critical reading of the manuscript. C.D.: study concept, funding and critical reading of the manuscript. S.C.M.: study concept, study supervision, planned the experiments, interpreted data, designed the figures and wrote the manuscript.

Additional Information

Supplementary information accompanies this paper at <https://doi.org/10.1038/s41598-019-51175-z>.

Competing Interests: The authors declare no competing interests.

Publisher's note Springer Nature remains neutral with regard to jurisdictional claims in published maps and institutional affiliations.



Open Access This article is licensed under a Creative Commons Attribution 4.0 International License, which permits use, sharing, adaptation, distribution and reproduction in any medium or format, as long as you give appropriate credit to the original author(s) and the source, provide a link to the Creative Commons license, and indicate if changes were made. The images or other third party material in this article are included in the article's Creative Commons license, unless indicated otherwise in a credit line to the material. If material is not included in the article's Creative Commons license and your intended use is not permitted by statutory regulation or exceeds the permitted use, you will need to obtain permission directly from the copyright holder. To view a copy of this license, visit <http://creativecommons.org/licenses/by/4.0/>.

© The Author(s) 2019